Carbon 246 (2026) 120900

Contents lists available at ScienceDirect

Carbon

journal homepage: www.elsevier.com/locate/carbon

Structure and spectroscopy of graphite monofluoride

Katherine M. Morton [a], A. Dominic Fortes [a], Daniel W. Nye [a], James D. Taylor [a], Luke L. Daemen [b], Alexander I. Kolesnikov [b], Victor R. Fanelli [b], Matthew B. Stone [b], Anibal J. Ramirez-Cuesta [b], Yongqiang Cheng [b], Valeri Leich [c], Peter W. Albers [d], Daniel M. Dawson [e], Stewart F. Parker [a,*]

[a] ISIS Pulsed Neutron and Muon Facility, STFC Rutherford Appleton Laboratory, Chilton, OX11 0QX, Oxon, UK
[b] Neutron Scattering Division, Oak Ridge National Laboratory, Oak Ridge, TN, 37831, USA
[c] Evonik Operations GmbH–Creavis, Paul-Baumann-Straße 1, 45772, Marl, Germany
[d] Evonik Technology & Infrastructure GmbH, 915 D115, Rodenbacher Chaussee 4, 63457, Hanau-Wolfgang, Germany
[e] School of Chemistry, University of St Andrews, North Haugh, St Andrews, Fife, KY16 9S, UK

ARTICLE INFO

Keywords:
Graphite monofluoride
Inelastic neutron scattering spectroscopy
Infrared spectroscopy
Raman spectroscopy
Neutron diffraction
Density functional theory

ABSTRACT

The structure of graphite monofluoride, $(CF)_n$, has been debated since its discovery in 1934. In this work, we investigate a commercial graphite monofluoride by vibrational spectroscopy (infrared, Raman and the first inelastic neutron scattering spectra of this material). The spectroscopy shows that the material contains unreacted graphite and the partially fluorinated product dicarbon fluoride, $(C_2F)_n$, We evaluate the previously proposed $P\bar{6}m2$ and $P\bar{3}m1$ structures using computational methods and find F···F contacts render the $P\bar{6}m2$ structure dynamically unstable. We propose two alternative structures, $Cmc2_1$ and $P6_3mc$, generated by displacement of one layer relative to another and find that $Cmc2_1$ is also dynamically unstable. The calculations are validated by comparison of calculated and observed INS spectra

1. Introduction

Graphite fluoride compounds, in particular graphite monofluoride ($(CF)_n$), are derivatives of graphite which have garnered significant attention due to their unique properties. Their low friction coefficients compared to pure graphite and high decomposition temperatures have enabled their commercial use as solid-state lubricants [1]. The excellent electrochemical properties of graphite fluoride compounds have also resulted in their use as cathode materials for lithium-ion batteries [2–5].

The first synthesis of a graphite monofluoride compound was reported in 1934 by Ruff and Bretschneider [6] via direct combination of graphite and fluorine at 420 °C without combustion. This yielded a grey solid, $(CF_x)_n$, where x was determined to be 0.92. Subsequent studies have given rise to substantial debate concerning the structure of the compound. In 1959, Rüdorff [7] proposed a structure based on X-ray diffraction, suggesting *trans*-linked cyclohexane rings in a chair conformation with fluorine atoms in the axial positions. Ebert et al. [8] indicated a boat-type structure from ^{19}F NMR measurements, but computational studies by Lazar et al. [9] found that the chair conformation is the most stable structure. More recently, Walder and Alam [10] found the boat and chair conformers can coexist as a form of disorder. Touhara et al. [11] determined $P\bar{6}m2$ as the space group, but Fujimoto [12] carried out a Rietveld analysis of XRD data and concluded that a $P\bar{3}m1$ structure was also a suitable fit for the data, and that both structures can co-exist due to the turbostratic properties of the carbon which causes disorder in the layers.

Although graphite monofluoride is defined by a 1:1 C:F stoichiometry, in practice it often coexists with structurally or chemically related phases. One such phase is poly(dicarbon monofluoride), $(C_2F)_n$, a common by-product formed during the fluorination of graphite in the synthesis of $(CF)_n$ [13]. Studies by Pischedda, Cavallari and co-workers have highlighted that fluorinated graphite compounds cannot be fully described by a single ordered phase [14–16]. Differences in C–F bonding character and local structure can account for some of the previous structural ambiguities, such as the coexistence of multiple conformations and the presence of different space groups. Despite being well characterised, the presence of $(C_2F)_n$ and other impurities can complicate the structural and spectroscopic analysis of $(CF)_n$, leading to additional features or peak broadening [13–19]. Therefore, accounting for

* Corresponding author.
E-mail address: stewart.parker@stfc.ac.uk (S.F. Parker).

https://doi.org/10.1016/j.carbon.2025.120900
Received 24 April 2025; Received in revised form 15 September 2025; Accepted 29 September 2025
Available online 30 September 2025

these additional phases is essential for the accurate characterisation of graphite monofluoride.

To date, insight into the structure of graphite monofluoride has relied on NMR [8,10,20], X-ray diffraction (XRD) [6,7,11,12,16,21–23], neutron diffraction (ND) [16], photoelectron spectroscopy [24] and computational investigations, in particular density functional theory (DFT) calculations [9,10,16,25,26]. Although XRD has been the predominant method, these studies have not fully resolved the structure, partly due to the difficulty obtaining a single crystal of $(CF)_n$. The vibrational spectroscopy remains relatively unexplored, with only a few Raman [23,27] and infrared [21,23,24] studies. Inelastic neutron scattering (INS) spectra have not been previously reported for any fluorinated graphite compounds, but offers distinct benefits, including the ability to detect all vibrational modes (due to access to the full Brillouin zone and no selection rules), high sensitivity to light elements (including C and F) and being highly penetrating (so it measures the bulk, rather than just the surface). In the present work, we have investigated the structure of commercial graphite monofluoride by XRD and neutron powder diffraction (NPD). We have also recorded new infrared and Raman spectra and report the first INS spectra of graphite monofluoride. The results are supported by density functional theory calculations of the structures.

2. Materials and methods

2.1. Graphite monofluoride

Graphite monofluoride (99 %) was purchased from ACS Materials. This material is stated to have a particle size of 1–10 μm and a F:C ratio of 0.8–1.1. A sample was dried under vacuum before use; the weight loss was less than 1 %.

2.2. X-ray powder diffraction

A Rigaku Smartlab XRD2 (Thin Film) was used to obtain powder X-ray diffraction (XRD) data. 1D high resolution measurements were carried out at room temperature, at a 0.08 °min^{-1} speed across a range of 5–80°. The crystallite size (D) was determined using the Scherrer equation, and the equation N = (D/d) + 1 (d = interlayer distance) was used to determine the average number of layers (N).

2.3. Surface area

The surface area was determined using the Brunauer–Emmett–Teller (BET) method. An Autosorb iQ-Chemi was used to dry the samples at 150 °C for 12 h and then to measure the surface area by adsorption of nitrogen gas at 77 K.

2.4. ^{13}C and ^{19}F solid state NMR spectroscopy

Solid-state NMR spectra were recorded on a Bruker Avance-III spectrometer equipped with a 9.4 T wide-bore superconducting magnet (^{13}C and ^{19}F Larmor frequencies of 100.6 and 376.4 MHz, respectively) and 1.3 mm magic angle spinning (MAS) probehead. The sample was rotated at the magic angle at a rate of 50–55 kHz. The ^{13}C spectrum was recorded using a rotor-synchronised spin-echo sequence with $\tau = \tau_r = 20$ ms and rotor-synchronised π pulses ($\nu_1 \approx 83$ kHz) applied to ^{19}F during acquisition. Signal averaging was carried out for 1008 transients with a recycle interval of 60 s. The ^{19}F NMR spectra were recorded using a rotor-synchronised spin-echo pulse sequence with $\tau = \tau_r = 18.2$ or 20 ms. Signal averaging was carried out for 16 or 64 transients with a recycle interval of 60 s. Chemical shifts are reported in ppm relative to Si $(CH_3)_4$ and CCl_3F using poly(tetrafluoroethylene) (PTFE) as a secondary solid reference (^{13}C $\delta = 111.3$ ppm, ^{19}F $\delta = -122.7$ ppm).

2.5. Vibrational spectroscopy

Room temperature infrared spectra were recorded with a Bruker Vertex70 FTIR spectrometer by attenuated total internal reflection (ATR) using a Bruker Diamond ATR accessory (256 scans, 4 cm^{-1} resolution across a range of 4000 to 50 cm^{-1} with 8 × zerofilling to improve the peak shape). An extended ATR correction (using the Bruker software) was applied to all measurements to correct for the wavelength dependent penetration depth.

Raman spectra were recorded with a Bruker Senterra Raman spectrometer at room temperature with 532 nm excitation, using 20 mW power with a 25 × 100 μm aperture and 3-5 cm^{-1} resolution. The sample was measured at three different positions for 3 × 10 s, and one position for 12 × 10s across the range 39–3704 cm^{-1}. Low temperature (10 K) Raman spectra were recorded with a previously reported [28] modified Renishaw InVia system using 532 and 785 nm excitation. Attempts to record spectra with 1064 nm excitation using a Bruker FT-Raman spectrometer (16 scans, 4 cm^{-1} resolution with 8 × zerofilling) were unsuccessful.

Inelastic neutron scattering (INS) spectra were recorded with the VISION [29] and SEQUOIA [30] spectrometers at the Spallation Neutron Source (Oak Ridge, TN, USA) [31]. The dried sample, ~5 g, was loaded into an indium wire sealed aluminium can and cooled to below 10 K for measurement. The two spectrometers have different operating characteristics as they are indirect and direct geometry spectrometers respectively, the differences are explained elsewhere [32]. VISION provides high quality spectra in the 0–2000 cm^{-1} region while SEQUOIA provides energy (E, cm^{-1}) and momentum (Q, $Å^{-1}$) resolved data in the 10–16000 cm^{-1} region. By selecting only the low Q data ($0 \leq Q \leq 10$ $Å^{-1}$), it is possible to access the 2000 - 4000 cm^{-1} region (where the C–H and O–H stretch modes occur) with reasonable resolution. Together, the spectrometers are highly complementary and enable vibrational spectra to be collected across the entire 0 - 4000 cm^{-1} range with good resolution and with no selection rules, so all the modes are, in principle, observable. VISION also has a large area detector in near backscattering that enables high quality neutron powder diffraction data to be collected simultaneously with the INS measurements. Low resolution neutron powder diffraction data are also present in the SEQUOIA data at $E = 0$.

2.6. Computational methods

Dispersion corrected periodic density functional theory (DFT-D) calculations were carried out with CASTEP (version 21.21) [33]. On-the-fly generated norm conserving pseudopotentials with a plane-wave cut-off of 840 eV were used with the PBE [34] functional with the Tkatchenko-Scheffler [35] dispersion correction scheme within the generalized gradient approximation (GGA). The Brillouin zone sampling of electronic states was performed with Monkhorst-Pack grids, details of the cells, the k-points and the convergence are given in Table S1 of the Electronic Supplementary Information (ESI). The equilibrium structure, an essential prerequisite for lattice dynamics calculations, was obtained by BFGS geometry optimization. Crystallographic Information Files (.cif) of all of the optimised structures are included in the ESI. Phonon frequencies were obtained by diagonalization of the dynamical matrix, computed using density-functional perturbation theory (DFPT) [36] to compute the dielectric response and the Born effective charges, and, from these, the mode oscillator strength tensor and infrared absorptivity were calculated. In addition to the calculation of transition energies at zero wavevector, for some systems, phonon dispersion was also calculated along high symmetry directions throughout the Brillouin zone. For this purpose, dynamical matrices were computed by DFPT on a regular grid of wavevectors throughout the Brillouin zone, and Fourier interpolation was used to extend the computed grid to the desired fine set of points along the high-symmetry paths [37]. Note that DFPT does not require the specification of supercells. The atomic displacements in each mode, which are part of the

CASTEP output, enable visualization of the modes in Materials Studio [38] to aid assignments and are also all that is required to generate the INS spectrum using the program AbINS [39] or OCLIMAX [40]. It is emphasised that, for the calculated spectra and dispersion curves shown, the transition energies have *not* been scaled.

3. Results and discussion

3.1. Structural studies

Fig. 1 shows the $P\bar{6}m2$ [11] (a) and $P\bar{3}m1$ [12] (c) structures. The individual layers in both structures are identical; the differences arise from how they are stacked. By sliding the second layer relative to the first, it is possible to generate a range of new structures. Two of these structures, $Cmc2_1$ and $P6_3mc$ are also shown in Fig. 1 (b and d respectively). The reasons for doing this will be discussed in Section 3.4.

BET analysis of the material reveals a surface area of 101 $m^2\ g^{-1}$. XRD indicates a crystallite size of ~3 nm and that there are approximately five layers present. Neutron and X-ray diffraction data are shown in Fig. 2 and are compared with the diffractograms calculated for the four structures shown in Fig. 1. Two key observations are apparent: all four structures produce broadly similar diffraction patterns for both ND and XRD, and while they all share similarities with the experimental data, none can fully reproduce it. As noted by other authors [11,12], this is undoubtedly a consequence of the turbostratic disorder of the layers. A weak peak at 1.9 $Å^{-1}$ (see also Fig. S1) is apparent in the experimental ND data that is not predicted by any of the models. This is assigned to the (002) reflection of a small amount of unreacted graphite [41].

3.2. Solid state ^{13}C and ^{19}F NMR spectroscopy

Fig. 3 shows the solid state ^{13}C and ^{19}F NMR spectroscopy of our graphite monofluoride sample. The NMR spectra have been comprehensively investigated by several authors [10,17]. Following the literature [24] the ^{13}C peaks are assigned as: graphite (137 ppm), edge terminating CF_2 (109 ppm), $(CF)_n$ + $(C_2F)_n$ (88 ppm) and C–C–F of $(C_2F)_n$ (55 ppm). The last of these is somewhat unexpected as 42 ppm is the accepted value. However, the vibrational spectroscopy clearly shows

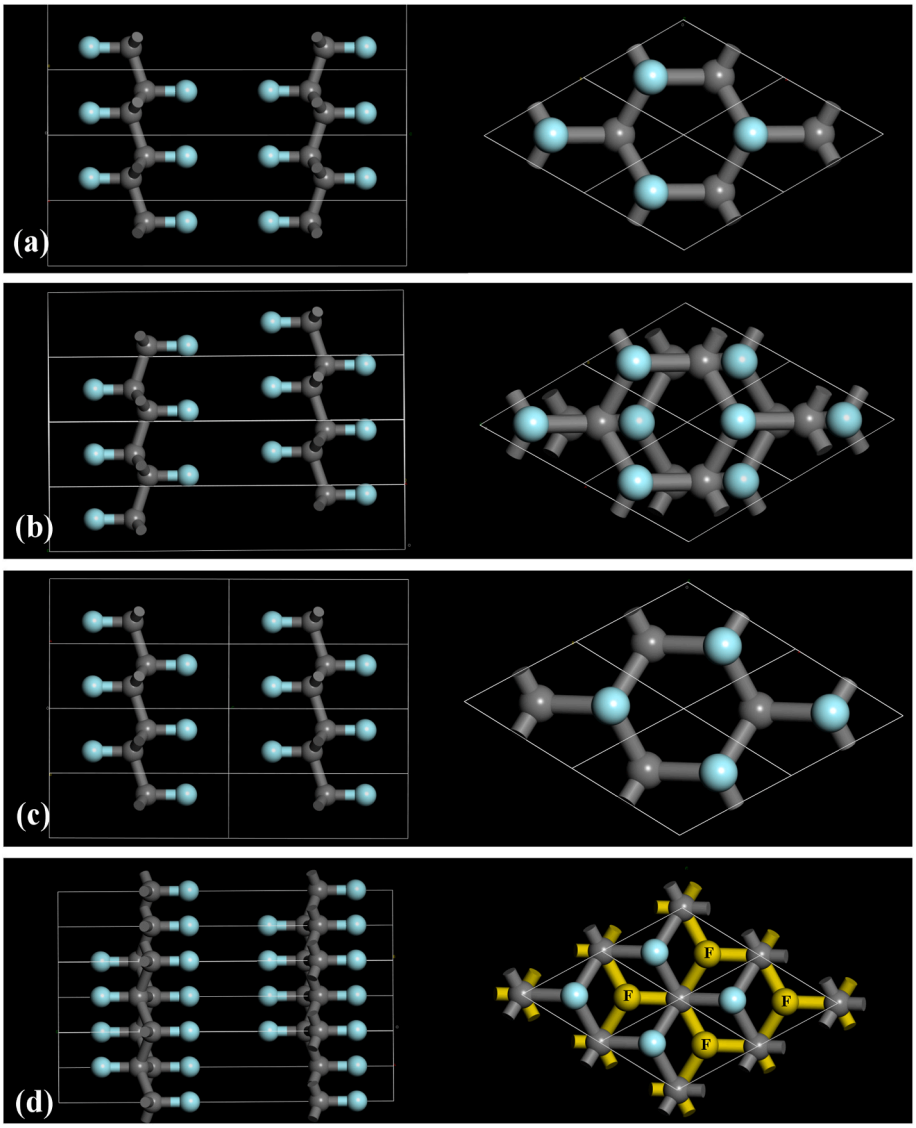

Fig. 1. Structural models of graphite monofluoride. Left hand side: view perpendicular to the longest axis, right hand side: view down the longest axis. (a) $P\bar{6}m2$, (b) primitive cell of $Cmc2_1$, (c) $P\bar{3}m1$ and (d) $P6_3mc$. In (d) the atoms in the second layer are shown in yellow for clarity, the fluorine atoms are labelled "F" and the carbon atoms are directly below the carbon atoms in the top layer. Key: grey = carbon, turquoise = fluorine. (For interpretation of the references to colour in this figure legend, the reader is referred to the Web version of this article.)

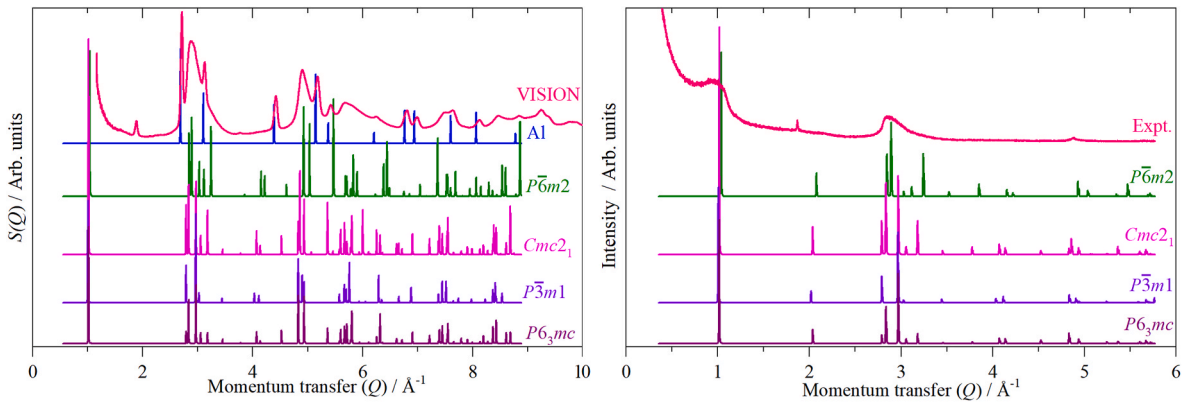

Fig. 2. Neutron (left) and X-ray (right) diffractograms of graphite monofluoride. The experimental spectrum is at the top in each case and below are the calculated diffractograms for the structures shown in Fig. 1. For the neutron data, the sample was held in an aluminium cell, the calculated ND pattern for this is also shown.

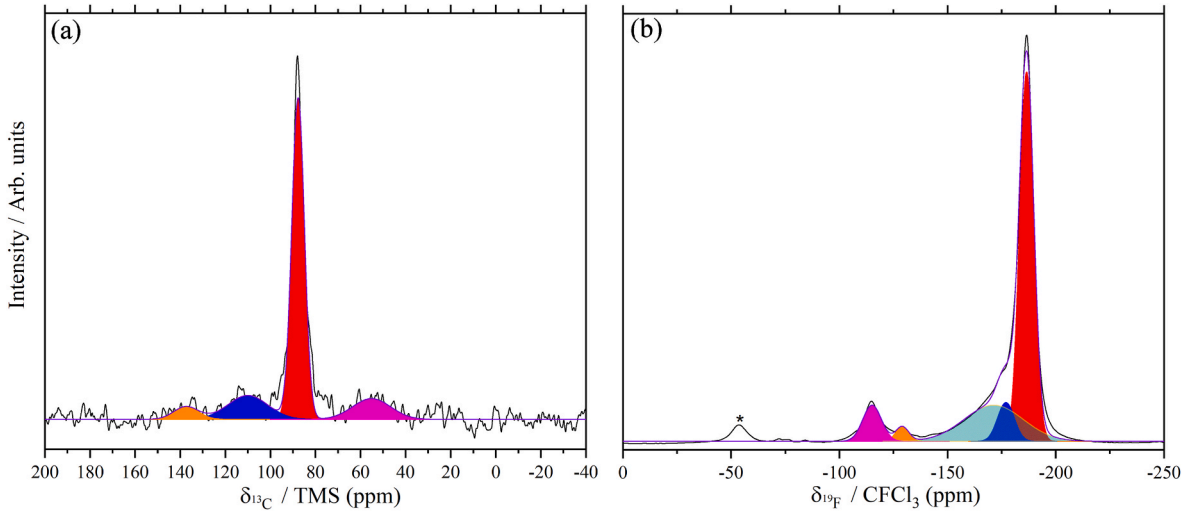

Fig. 3. Room temperature solid state NMR spectroscopy of graphite monofluoride: (a) ^{13}C and (b) ^{19}F. In (b) the peak marked with * is a spinning side band (see Fig. S2).

the presence of $(C_2F)_n$, (see section 3.5). The ^{19}F peaks are assigned as [17]: edge terminating CF_2 (−115 ppm and −129 ppm), $(C_2F)_n$ with $(C_2F)_n$ neighbours, (−171 ppm), $(C_2F)_n$ with $(CF)_n$ neighbours, (−177 ppm) and $(CF)_n$ (−186 ppm). The chemical shifts of $(C_2F)_n$ with $(C_2F)_n$ and $(CF)_n$ neighbours differ from the literature values (−178 and −183 respectively [24]) but the positions are determined by curve fitting (both here and in Ref. [17]), so some difference in position for weak, strongly overlapped species is not unexpected.

Based on the areas of the 88 and 55 ppm peaks in the ^{13}C spectrum, we find that there is ~20 % $(C_2F)_n$ present in the sample with an overall F/C ratio of 0.84. Both of these are lower bounds; the data are noisy and the peak assigned to C–C–F of $(C_2F)_n$ is not at the literature value, so may be another species. It is clear that the majority species (>80 %) present is $(CF)_n$ with some graphite and $(C_2F)_n$.

3.3. Vibrational spectroscopy

Fig. 4 shows the infrared and INS spectra of graphite monofluoride. The infrared spectrum (Fig. 4a) closely resembles those previously reported for stoichiometric (or nearly so) samples from both commercial [42] and in-house preparations [21,23]. The very strong band at 1196 cm^{-1} is assigned as the C–F stretch of carbon atoms bonded to three adjacent carbon atoms i.e. as shown in Fig. 1. While this is the usual assignment, what has not been noted before is that this is unusually high for a C–F stretch; in a series of monofluoro *n*-alkanes [43] (C4, C5, C6) the C–F stretch occurred in the 1000–1100 cm^{-1} range. In the hydrogenated analogue of graphite monofluoride, (hydrogenated crystalline graphite, hydrographite or graphane [44,45]) the ratio of the C–H stretching mode (2850 cm^{-1}) to the C–D stretch (2080 cm^{-1}) is 1.36, which closely follows the square root of the ratio of the reduced masses of C–D and C–H. If we assume the force constant between C and F is the same as that between C and H (or D), then the expected C–F frequency should be 1002 cm^{-1}, also in good agreement with [23]. This suggests that the C–F bond in graphite monofluoride is unusually strong.

The second strongest band is at 328 cm^{-1}, this was previously [23] assigned as an edge-terminating CF_2 deformation mode. However, an assignment to the C–F bending mode is more reasonable on intensity grounds.

In addition to these bands, there are weak features in the infrared spectrum at 1566, 1358, 1251, 976, 945 and 551 cm^{-1}. The band at 1358 cm^{-1} has been assigned [23,24] as a C–F stretching mode of edge-terminating CF_2 groups. By comparison with the spectra and assignments for perfluorocyclohexane [46], PTFE [47] and 2,2-difluoropropane [48] we agree with this view. We will discuss this in more detail in the section on Computational Studies. The 551 cm^{-1} band is assigned as the CF_2 scissors mode. The doublet at 976 and 945 cm^{-1} has been seen in other work [22] but not assigned. Perfluorocyclohexane [46] has a very strong doubly degenerate E_u mode at 986 cm^{-1} that is assigned as a C–C stretch and we adopt this assignment for the 976 cm^{-1} mode. .The 945 cm^{-1} band will be discussed in section 3.5.

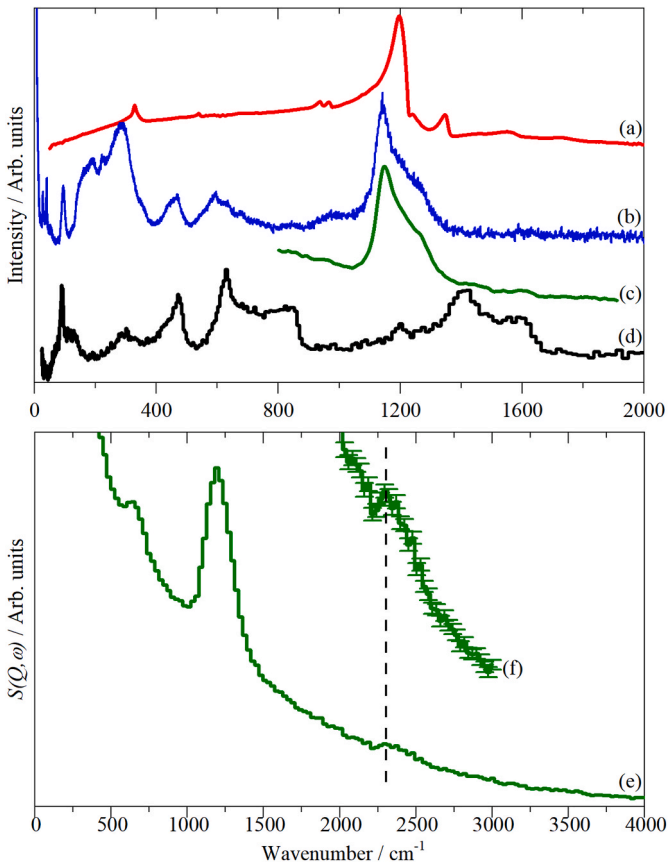

Fig. 4. Vibrational spectra of graphite monofluoride. (a) Infrared at room temperature, INS at 10 K recorded with (b) VISION and (c) SEQUOIA (250 meV incident energy) spectra of graphite monofluoride. (d) INS (at 10 K) spectrum of graphite recorded with TOSCA [49], (e) INS spectrum of graphite monofluoride recorded with SEQUOIA (650 meV incident energy) (spectra recorded with other incident energies are shown in Fig. S3) and (f) × 5 ordinate expansion of (e), the error bars are also shown. The dashed line in the lower figure indicates the first overtone of the overlapping C–C and C–F stretch.

The most striking feature of the INS spectrum of graphite monofluoride recorded on VISION, Fig. 4b, is its stark contrast to the infrared spectrum of the same material. There are several reasons for this. The intensity of an INS feature is determined by both the amplitude of motion of the atoms in the mode and the scattering cross section of the atoms. Given that carbon and fluorine have similar masses, 12 and 19 amu, the amplitudes of motion will be similar. The total scattering cross section's are also similar (C = 5.551 b, F = 4.018 b, 1 b = 10^{-28} m^2), so together these two factors ensure that C and F will both contribute significantly to the observed spectrum. In contrast, the infrared spectrum is dominated by modes involving fluorine. In addition, the peak shapes of the INS bands exhibit considerable structure compared to the infrared spectrum. Both of these observations (the difference in peak maximum and the band shape) are evidence for strong vibrational dispersion (variation of peak position with wavevector) in graphite monofluoride. INS is sensitive to all wavevectors across the entire Brillouin zone, whereas infrared and Raman spectra are observed at the Brillouin zone centre (the Γ-point). This will be supported in Section 3.3 Computational studies.

Neutrons are highly penetrating because they are scattered by the atomic nuclei, rather than the electrons. Thus, most of matter is empty space to a neutron. As a result, unless the surface area is very large, the spectra are representative of the bulk of the sample. This is the case here; the surface area is modest (101 m^2 g^{-1}), so the edge terminating species are not seen in the INS spectra.

The INS spectrum recorded with SEQUOIA using 250 meV incident energy (~2000 cm^{-1}) is shown in Fig. 4c (spectra recorded with other incident energies are shown in Fig. 4e and Fig. S3) and the similarity to the VISION spectrum is clear. However, weak features at 1425 and 1600 cm^{-1} are present and comparison with the INS spectrum of graphite [49], Fig. 4d, suggests they should be assigned to unreacted graphite.

The spectrum recorded with SEQUOIA using 650 meV incident energy(~5240 cm^{-1}) is shown in Fig. 4e. There are no modes in the C–H or O–H stretch region above 2800 cm^{-1}, consistent with the stated composition ($CF_{0.8-1.1}$, i.e. there is no H present). There is a very weak feature at 2350 cm^{-1}, which we assign as the first overtone of the overlapping C–C and C–F stretch modes (Fig. 4f). Since this is close to twice that of the fundamental mode (2 × 1196 = 2392 cm^{-1}), this indicates a harmonic, or nearly so, system (overtones and combinations are allowed modes in INS spectroscopy).

The Raman spectrum of graphite monofluoride is shown in Fig. 5. Fig. 5a, the spectrum at room temperature, closely resembles previous work [22,50]. The spectrum recorded at 10 K with baseline correction to remove the fluorescence background, Fig. 5b, consists of two prominent peaks at 1545 and 1307 cm^{-1} and two weaker peaks at 1420 and 1184 cm^{-1}. The peaks at 1545 and 1307 cm^{-1} are assigned as the G and D bands of graphite [51]. These peaks are only present if there is some residual, unreacted graphite present in the sample, consistent with the ND results of Fig. 2 and the SEQUOIA data in Fig. 4c. This is also in agreement with the dark grey colour of the material, as it has been shown [13,23,25] that as the material approaches being stoichiometric $(CF)_n$, its colour progressively lightens from black to white. The presence of graphite would also account for the 1566 cm^{-1} infrared band in Fig. 5a. The amount of unreacted graphite must be small and highlights the high sensitivity of Raman spectroscopy to graphite. The 1420 cm^{-1} Raman band is probably due to amorphous carbon. The weak band at 1184 cm^{-1} is close to that seen in the infrared spectrum for the C–F stretch and we assign it as such. This is the first time that this mode has been seen in the Raman spectrum of graphite monofluoride.

3.4. Computational studies

In this section, we use periodic density functional theory calculations (DFT) to investigate the relative stability of the structures and to support the vibrational assignments given in the previous section. Previous DFT studies on a variety of fluorinated carbons are reviewed in Ref. [2].

From the diffraction studies all of the structures in Fig. 1 could be present in graphite monofluoride. This is because the in-plane structure is the same in all cases and they only differ in the interlayer ordering as a result of the turbostratic disorder.

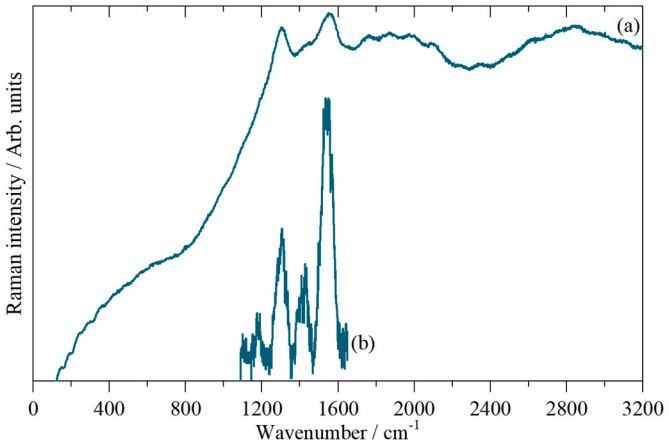

Fig. 5. Raman spectra of graphite monofluoride. (a) recorded with 532 nm excitation at room temperature and (b) recorded at 10 K after baseline correction.

Table 1 shows the results of the DFT calculations (a more complete version is shown in Table S2) and it can be seen that the energy differences between the structures are tiny and generally less than DFT accuracy [52] (typically 5–10 kJ mol^{-1}, 1 kJ mol^{-1} = 10 meV). This is likely a consequence of the energetics being dominated by the in-plane structure, which is common to all of the structures, with the weak inter-layer forces only making a small contribution.

However, a more intriguing observation is that two of the structures are dynamically unstable as evidenced by the presence of imaginary modes at the Brillouin zone Γ-point. Inspection of the mode animations reveals that the two imaginary modes in $P\bar{6}m2$ are inter-layer shearing modes. In this structure, the shortest inter-layer contact is F···F at 2.807 Å, which is significantly less than twice the van der Waals radius of fluorine (2 × 1.47 = 2.94 Å). If one of the layers is translated by 0.7 Å, so that the F···F distance increases to 3.037 Å, the space group becomes $Cmc2_1$. This has one imaginary mode, which is also an inter-layer shearing mode. If the second layer is further translated such that one of the C–F bonds is directed to the centre of the hexagon of C–C bonds in the layer above (see Fig. 1d), the space group becomes $P6_3mc$ with all real modes across the entire Brillouin zone, Fig. 6a. We find that the $P\bar{3}m1$ structure also has all real modes across the entire Brillouin zone, Fig. 6b. In this structure the C–F bonds point to a carbon atom in the layer above. This suggests that structures where there are F···F interactions (i.e., $P\bar{6}m2$ and $Cmc2_1$) are likely to be disfavoured and probably only occur as defects.

A stringent test of a model is how well it reproduces the experimental INS spectrum. Fig. 7 shows a comparison of the INS spectra calculated for the $P6_3mc$ and $P\bar{3}m1$ structures at the Brillouin zone centre (Γ-point) and for the full dispersion calculation across the entire Brillouin zone.

It is apparent that the Γ-point calculation ((c) in both parts of Fig. 7) does not describe the spectrum well. Inspection of the dispersion curves in Fig. 6 shows that all of the modes are strongly dispersive and since the INS spectrum can be considered to be a weighted projection of the dispersion curves on the wavenumber axis, this is unsurprising.

Both complete dispersion calculations reproduce the experimental spectrum well. The C–C and C–F stretching modes at 1000–1200 cm^{-1} are slightly underestimated but the overall shape of each of the features is reasonably well reproduced. The best match, Fig. 7b, is a broadened calculated spectrum. This is because there are only a limited number of *k*-points calculated (in order to make the calculation tractable) and the real material is not a perfect, ordered structure. Broadening the spectrum is a crude, but effective, way to compensate for both effects.

Close inspection shows that the $P6_3mc$ structure is a slightly better match, but the differences between it and the $P\bar{3}m1$ structure are small. This is again a consequence of the strong in-plane bonding, which is common to both structures.

Decomposition of the calculated INS spectra in Fig. 7 for the $P6_3mc$ structure into the neutron weighted vibrational density of states (VDOS) of carbon and fluorine provides an explanation for the difference in peak maxima for the infrared and INS spectra (see Fig. 4a and b). From Fig. 8, it can be seen that most of the strong feature at 1000–1400 cm^{-1} is accounted for by the strongly dispersive C–C stretch modes and that the dispersive C–F stretch modes make only a minor contribution (Fig. 8b and c). For the modes at the Brillouin zone Γ-point, those associated with the C–F stretch are at lower energy than the C–C stretch modes but still occur higher than the peak in the neutron weighted VDOS. As the infrared spectrum is only active at the Γ-point, it follows that the INS and infrared spectra will show different peak maxima, with that of the infrared being at higher wavenumber, exactly as seen in Fig. 4. The same is also true for the $P\bar{3}m1$ structure and this is shown in Fig. S4.

In the same way that graphene is related to graphite, fluorographene [53] is the single layer version of graphite monofluoride. Computational studies [54,55] of fluorographene find the chair conformation to be lowest in energy, exactly as for graphite monofluoride. The vibrational

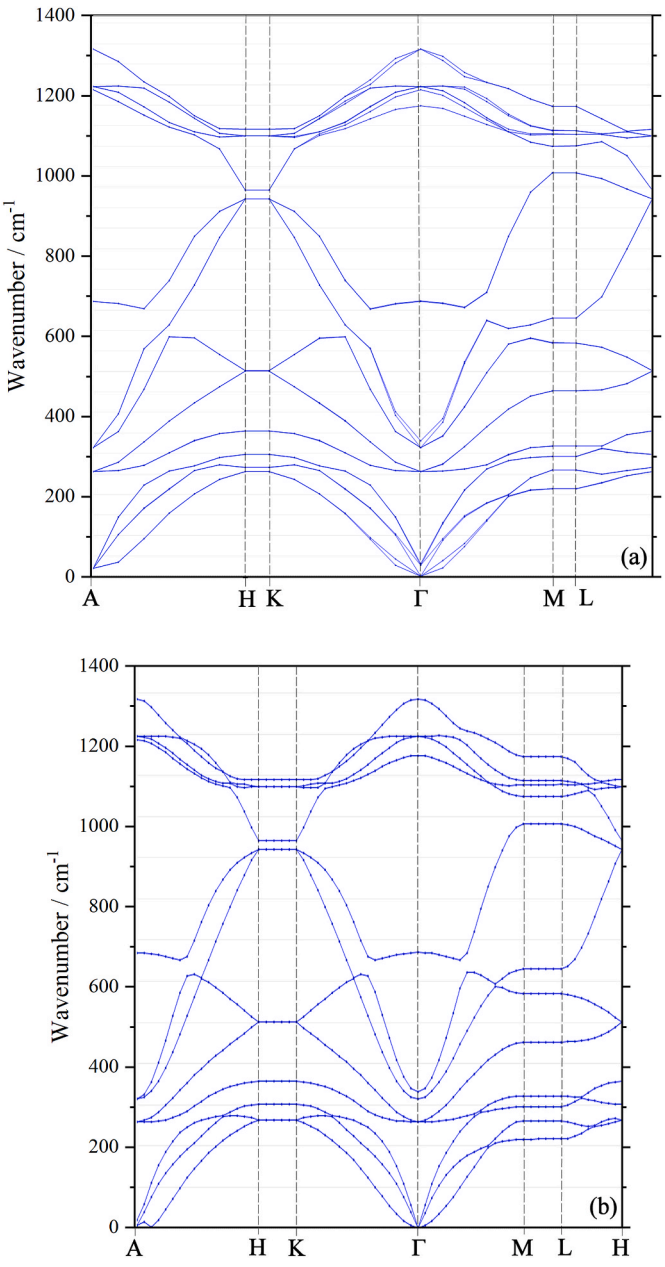

Fig. 6. Dispersion curves for graphite monofluoride: (a) $P6_3mc$ and (b) $P\bar{3}m1$ structure.

Table 1
C–C and C–F bond distances, the energies per CF unit of the structures studied and the number of imaginary modes at the Brillouin zone Γ-point.

Structure	C–C[a] /Å	C–F /Å	Relative energy per CF unit /meV	No. of imaginary modes at Γ-point
$P\bar{6}m2$	1.552 (1.557)	1.375 (1.289)	21.5	2
$Cmc2_1$	1.580	1.376	0.8	1
$P\bar{3}m1$	1.580 (1.585)	1.376 (1.349)	1.4	0
$P6_3mc$	1.580	1.376	0.0	0
PDF X-ray	(1.574)	(1.361)		
PDF neutron	(1570)	(1.330)		

[a] Values in brackets are experimental values from Ref. [11] ($P\bar{6}m2$) [12], ($P\bar{3}m1$) and [13] (PDF X-ray and PDF neutron).

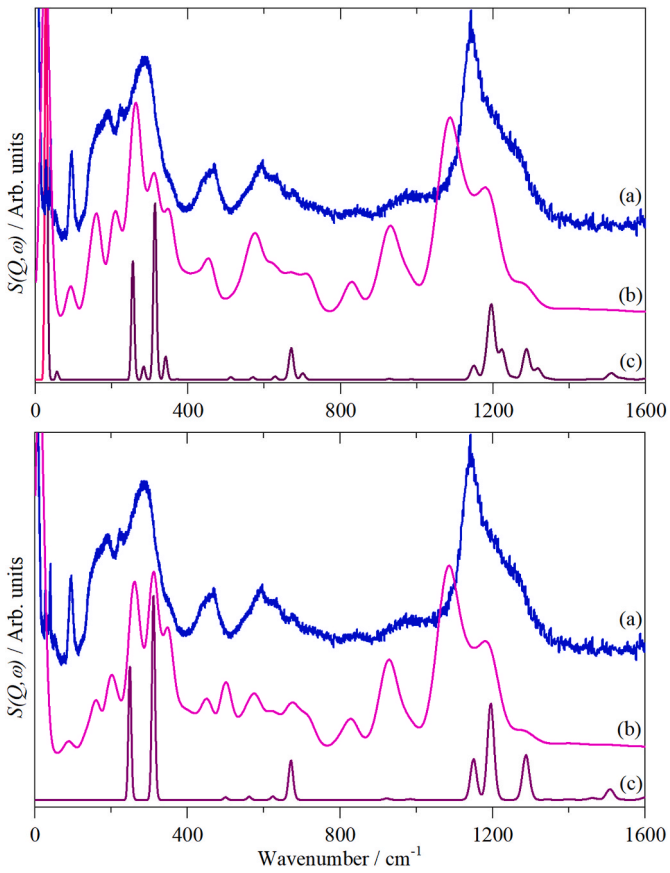

Fig. 7. Comparison of experimental and calculated VISION INS spectra of graphite monofluoride. The top part corresponds to the $P6_3mc$ and bottom to the $P\bar{3}m1$ structure. For both parts (a) is the observed INS spectrum, (b) is from a calculation of the complete Brillouin zone that has been broadened and (c) is a calculation at the Brillouin zone Γ-point at VISION's resolution.

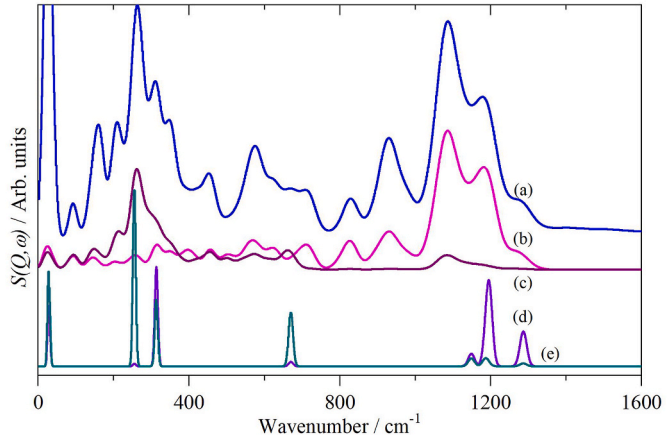

Fig. 8. Calculated INS spectrum and vibrational density of states (VDOS) for graphite monofluoride in the $P6_3mc$ structure. (a) is the calculated INS spectrum, (b) and (c) are the neutron weighted VDOS for carbon and fluorine respectively from a calculation of the complete Brillouin zone that has been broadened, (d) and (e) are the VDOS for carbon and fluorine respectively from a calculation at the Brillouin zone Γ-point at VISION's resolution.

modes are strongly dispersive and the VDOS is very similar: the C–C stretch modes dominate the 1000–1400 cm^{-1} region and the C–F bend modes the 1000–1400 cm^{-1} region, as found here for graphite monofluoride.

The mode visualisations enable the experimental INS spectrum to be assigned: the broad feature at 1100–1300 cm^{-1} are the C–C stretch modes with the C–F stretch modes only making a minor contribution. The structured bands at 500–800 cm^{-1} are the ring bending modes and the broad, intense band at 200–400 cm^{-1} is the C–F bending modes. The complex shapes arise from the strong vibrational dispersion present in all the modes, see Fig. 6.

Comparison of the SEQUOIA data with that generated from the calculated $P\bar{3}m1$ structure shows some interesting features (Fig. 9). The calculated spectra reproduce the structure apparent in the experimental spectra, particularly the "arches" that result from sampling neighbouring Brillouin zones. This is a result of both carbon and fluorine being almost purely coherent scatterers.

3.5. Dicarbon monofluoride, $(C_2F)_n$

The graphite monofluoride used in this work is a commercial material with a stated F:C ratio of 0.8–1.1. The neutron diffraction, NMR and INS studies show that there is unreacted graphite present (Fig. 2 (left), 3a, 4c, S1) and also partially reacted material present i.e. dicarbon monofluoride, $(C_2F)_n$. The bands at 1340 and 946 cm^{-1} in the infrared spectrum have been previously assigned to this phase [17] and they are present in our material. Comparison of our infrared spectrum, Fig. 4a, with that of a series of fluorinated graphites that have been characterised by ^{13}C NMR [17] and using the correlation proposed between the ratio of the intensities of the 1340 and 1200 cm^{-1} and the 940 and 1200 cm^{-1} infrared bands, suggests that our sample contains ~10 % $(C_2F)_n$, in general agreement with the 13C NMR result (~20 %). Both methods ignore the graphite content, so the wt% in the sample would be less than this. As noted earlier, INS measures the bulk, so is relatively insensitive to impurities. At the 10 % level, $(C_2F)_n$ is unlikely to be seen in the INS spectrum. Fig. S5 compares the experimental INS spectrum with that calculated for the $P\bar{3}m1$ structure of $(C_2F)_n$, it can be seen that the match is much poorer than that seen in Fig. 7. Fig. S6 shows a comparison of the calculated spectrum of $(CF)_n$ with that with 10 % $(C_2F)_n$ included. It is apparent that there is little difference between the two.

3.6. Edge termination in carbon monofluoride

Previous work [17] has shown that in samples with a high content of $(C_2F)_n$ the 940 and 1340 cm^{-1} infrared bands have nearly 1:1 intensity, in contrast to the ~1:10 seen in our material. This suggests that there is an additional contribution to the 1340 cm^{-1} band. As the material has finite particle size, it follows that there must be edges and to avoid dangling modes these must be terminated. These are most likely to be CF_2 groups, as shown by ^{13}C and ^{19}F NMR studies [10,17] and our data (Fig. 3).

To investigate the effects of edge termination, we took the $P\bar{3}m1$ model and cleaved it along (1 0 0). This resulted in dangling bonds that were then terminated with fluorine, to generate surface CF_2 groups (see Fig. 10 top part for the structure). This is not intended as a realistic model because the ratio of edge terminating CF_2 groups to bulk C–F bonds is too high. (The average platelet size is ~3 nm, the length of the system shown is ~1.6 nm. Increasing this to 3 nm would make this computationally expensive). As noted earlier, the INS spectra are not sensitive to the surface termination, but the infrared spectra are. Fig. 10a–c shows the experimental infrared spectrum and those calculated for the infinite model and with terminating CF_2 groups.

For the infinite structure, the mode visualisations confirm our assignment (Section 3.2) that the band at 328 cm^{-1} is the C–F bending mode. Comparison of the calculated spectrum for the infinite structure with that with terminating CF_2 groups (Fig. 10b and c respectively) shows additional bands that largely agree with those seen in the experimental spectrum. The highest energy band in the spectra for the structure with terminating CF_2 groups is at 1283 cm^{-1} and the mode

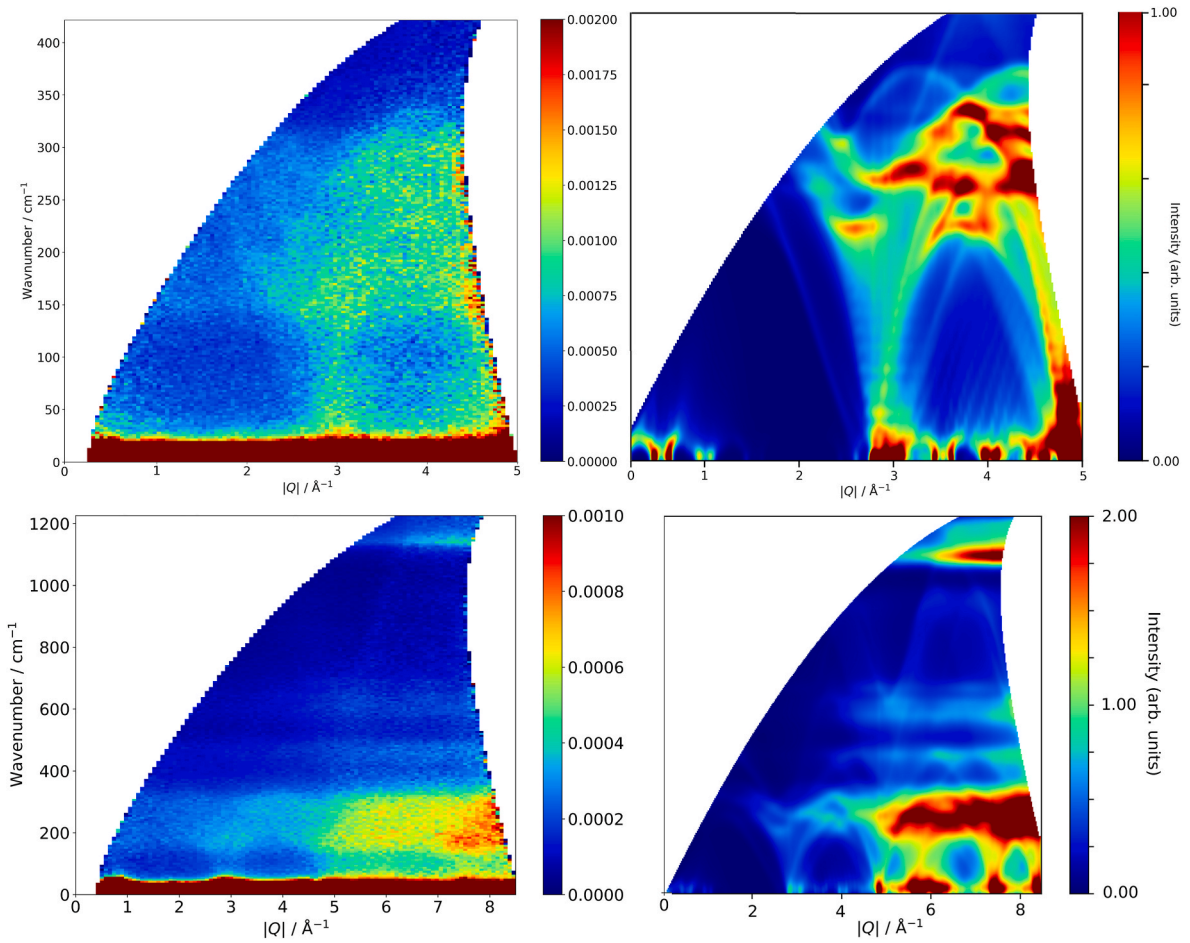

Fig. 9. Comparison of experimental and calculated SEQUOIA INS spectra of graphite monofluoride. Experimental (left) and calculated (right) SEQUOIA INS spectra of graphite monofluoride for the $P\bar{3}m1$ structure. Top: with 444 cm^{-1} incident energy, bottom: with 1250 cm^{-1} incident energy.

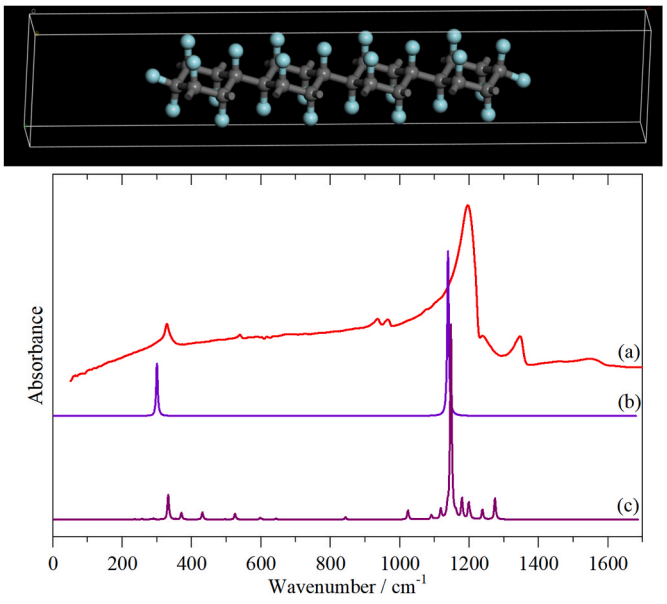

Fig. 10. Top: $P\bar{3}m1$ model cleaved along (1 0 0) and terminated with fluorine to generate surface CF_2 groups. Bottom: comparison of: (a) experimental and (b) calculated infrared spectra of graphite monofluoride with the $P\bar{3}m1$ structure and (c) the CF_2 terminated structure shown in the top part.

visualization shows that this is the symmetric (in-phase) C–F stretch of CF_2 groups. This is in agreement with 2,2-difluoropropane [47], but disagrees with perfluorocyclohexane [45] and PTFE [46], where the asymmetric (out-of-phase) stretch is at higher energy. The calculations indicate that the asymmetric stretch is around 1150 cm^{-1}, so we assign the weak band at 1251 cm^{-1} to this mode. The calculations confirm that the 976 cm^{-1} band is a

C–C stretch and the CF_2 scissors as the 551 cm^{-1} band (495 cm^{-1} calculated). The other three modes associated with the CF_2 groups (rock, wag, twist) are all predicted to have low infrared intensities so are not seen.

4. Conclusions

In this work we have investigated the structure and vibrational spectroscopy of commercial graphite monofluoride by experimental and computational methods. Two structures have been previously proposed for graphite monofluoride, $P\bar{6}m2$ and $P\bar{3}m1$; our lattice dynamics calculations show that the former is dynamically unstable. We have generated two new structures by displacement of one layer relative to another, $Cmc2_1$ and $P6_3mc$. Again, the former is dynamically unstable. The common feature of these dynamically unstable structures is the presence of F···F contacts; the stable structures align as F···C ($P\bar{3}m1$) and with the fluorine atoms pointing to the centre of the carbon hexagons ($P6_3mc$).

The infrared spectra are dominated by the C–F stretch and bend modes, weak features due to $(C_2F)_n$ and CF_2 edge terminating groups are also present and these are assigned with the aid of DFT calculations. We

have also measured the INS spectra of graphite monofluoride for the first time, using two complementary spectrometers, VISION and SEQUOIA. Comparison of the observed and calculated INS spectra show that both the $P\bar{3}m1$ and $P6_3mc$ structures provide good matches to the spectra. This is a consequence of the spectra being dominated by the in-plane structure which is common to all models (note that fluorination of graphite results in interlayer expansion by about 84 %). The INS spectra show that there is extensive vibrational dispersion present in graphite monofluoride which is confirmed by DFT calculations of the complete Brillouin zone. Neutron diffraction, ^{13}C solid state NMR, Raman and INS spectra show the presence of some residual unreacted graphite, consistent with the dark grey colour of the material. There is also some partially reacted graphite present as dicarbon monofluoride.

CRediT authorship contribution statement

Katherine M. Morton: Writing – review & editing, Writing – original draft, Investigation. **A. Dominic Fortes:** Writing – review & editing, Investigation. **Daniel W. Nye:** Writing – review & editing, Investigation. **James D. Taylor:** Writing – review & editing, Investigation. **Luke L. Daemen:** Writing – review & editing, Funding acquisition. **Alexander I. Kolesnikov:** Writing – review & editing, Investigation. **Victor R. Fanelli:** Writing – review & editing, Investigation. **Matthew B. Stone:** Writing – review & editing, Investigation. **Anibal J. Ramirez-Cuesta:** Writing – review & editing, Investigation. **Yongqiang Cheng:** Writing – review & editing, Investigation. **Valeri Leich:** Writing – review & editing, Funding acquisition, Conceptualization. **Peter W. Albers:** Writing – review & editing, Funding acquisition, Conceptualization. **Daniel M. Dawson:** Writing – review & editing, Investigation. **Stewart F. Parker:** Writing – review & editing, Writing – original draft, Investigation, Funding acquisition, Conceptualization.

Declaration of competing interest

The authors declare that they have no known competing financial interests or personal relationships that could have appeared to influence the work reported in this paper.

Acknowledgements

This research used resources at the Spallation Neutron Source, a DOE Office of Science User Facility operated by the Oak Ridge National Laboratory. Computing resources (time on the SCARF computer cluster for the CASTEP calculations) was provided by STFC's e-Science facility. This research has been performed with the aid of facilities at the Research Complex at Harwell, including the FT-Raman and UV–vis spectrometers. The authors would like to thank the Research Complex for access and support to these facilities and equipment.

Appendix A. Supplementary data

Supplementary data to this article can be found online at https://doi.org/10.1016/j.carbon.2025.120900.

References

[1] R.L. Fusaro, H.E. Sliney, Graphite fluoride $(CF_x)_n$ - a new solid lubricant, Tribol. Trans. 13 (1970) 56–65.
[2] N. Sharma, M. Dubois, K. Guérin, V. Pischedda, S. Radescu, Fluorinated (Nano) Carbons: CF_x electrodes and CF_x-Based batteries, Energy Technol. 9 (2021) 2000605.
[3] H.F. Hunger, G.J. Heymach, Cathodic discharge of graphite intercalation compounds in organic electrolytes, J. Electrochem. Soc. 120 (1973) 1161–1168.
[4] N. Watanabe, M. Fukuda, US Patent 3536532, 1970.
[5] A. Hamwi, K. Guérin, M. Dubois, in: T. Nakajima, H. Groult (Eds.), Fluorinated Materials for Energy Conversion, Elsevier, 2005, pp. 369–395.
[6] O. Ruff, O. Bretschneider, Die Reaktionsprodukte der verschiedenen Kohlenstoffformen mit Fluor II (Kohlenstoff-monofluorid), Z. Anorg. Allg. Chem. 217 (1934) 1–18.
[7] W. Rüdorff, in: H.J. Emeléus, A.G. Sharpe (Eds.), Advances in Inorganic Chemistry and Radiochemistry, Elsevier, 1959, pp. 223–266.
[8] L.B. Ebert, J.I. Brauman, R.A. Huggins, Carbon monofluoride, Evidence for a structure containing an infinite array of cyclohexane boats, J. Am. Chem. Soc. 96 (1974) 7841–7842.
[9] P. Lazar, E. Otyepková, F. Karlický, K. Čépe, M. Otyepka, The surface and structural properties of graphite fluoride, Carbon 94 (2015) 804–809.
[10] B.J. Walder, T.M. Alam, Modes of disorder in poly(carbon monofluoride), J. Am. Chem. Soc. 143 (2021) 11714–11733.
[11] H. Touhara, K. Kadono, Y. Fujii, N. Watanabe, On the structure of graphite fluoride, Z. Anorg. Allg. Chem. 544 (1987) 7–20.
[12] H. Fujimoto, Structure analysis of graphite fluoride by the Rietveld method, Carbon 35 (1997) 1061–1065.
[13] Y. Kita, N. Watanabe, Y. Fujii, Chemical composition and crystal structure of graphite fluoride, J. Am. Chem. Soc. 101 (1979) 3832–3841.
[14] V. Pischedda, S. Radescu, M. Dubois, N. Batisse, F. Balima, C. Cavallari, L. Cardenas, Experimental and DFT high pressure study of fluorinated graphite $(C_2F)n$, Carbon 114 (2017) 690–699.
[15] C. Cavallari, S. Radescu, M. Dubois, N. Batisse, H. Diaf, V. Pischedda, Tuning C–F bonding of graphite fluoride by applying high pressure: experimental and theoretical study, J. Phys. Chem. C 124 (2020) 24747–24755.
[16] C. Cavallari, M. Brunelli, S. Radescu, M. Dubois, N. Batisse, G.B.M. Vaughan, H. E. Fischer, V. Pischedda, Structural and electronic changes in graphite fluorides as a function of fluorination rate: an XRS, PDF and DFT study, Carbon 147 (2019) 1–8.
[17] V. Nesvizhevsky, K. Henry, L. Dauga, B. Clavier, S. Le Floch, E. Lychagin, A. Muzychka, A. Nezvanov, V. Pischedda, C. Teander, K. Turlybekuly, S. Radescu, B. Vigolo, S. Cahen, C. Hérold, J. Ghanbaja, K. Zhernenkov, M. Dubois, Poly (dicarbon monofluoride) $(C_2F)n$ bridges the neutron reflectivity gap, Carbon 227 (2024) 119249.
[18] Y. Sato, K. Itoh, R. Hagiwara, T. Fukunaga, Y. Ito, Short-range structures of poly (dicarbon monofluoride) (C_2F) and poly(carbon monofluoride) (CF), Carbon 42 (2004) 2897–2903.
[19] M. Dubois, J. Giraudet, K. Guérin, A. Hamwi, Z. Fawal, P. Pirotte, F. Masin, EPR and solid-state NMR studies of poly(dicarbon monofluoride) $(C_2F)n$, J. Phys. Chem. B 110 (2006) 11800–11808.
[20] A.M. Panich, Nuclear magnetic resonance study of fluorine–graphite intercalation compounds and graphite fluorides, Synth. Met. 100 (1999) 169–185.
[21] A. Hamwi, M. Daoud, J.C. Cousseins, Graphite fluorides prepared at room temperature 1. Synthesis and characterization, Synth. Met. 26 (1988) 89–98.
[22] V. Gupta, T. Nakajima, Y. Ohzawa, B. Žemva, A study on the formation mechanism of graphite fluorides by Raman spectroscopy, J. Fluor. Chem. 120 (2003) 143–150.
[23] R.J. Lagow, R.B. Badachhape, J.L. Wood, J.L. Margrave, Synthesis of "superstoichiometric" poly(carbon monofluoride), J. Am. Chem. Soc. 76 (1974) 2628–2629.
[24] D.T. Clark, J. Peeling, Applications of ESCA to polymer chemistry. XII. Structure and bonding in commercially produced fluorographites, J. Polym. Sci. Polym. Chem. 14 (1976) 2941–2967.
[25] J.C. Charlier, X. Gonze, J.P. Michenaud, First-principles study of graphite monofluoride (CF)*n*, Phys. Rev. B 47 (1993) 16162–16168.
[26] H. Zhao, J.K. Pu, M.K. Phuthi, C. Eschler, Y.-M. Chiang, V. Viswanathan, Effect of weakened bond covalence on the electronic, thermal, and elastic properties of disordered graphite monofluorides, J. Phys. Chem. C 129 (2025) 10731–10743.
[27] V. Gupta, T. Nakajima, B. Žemva, Raman scattering study of highly fluorinated graphite, J. Fluor. Chem. 110 (2001) 145–151.
[28] M.A. Adams, S.F. Parker, F. Fernandez-Alonso, D.J. Cutler, C. Hodges, A. King, Simultaneous neutron scattering and Raman scattering, Appl. Spec. 63 (2009) 727–732.
[29] https://neutrons.ornl.gov/vision Accessed on 9 January 2025.
[30] G.E. Granroth, A.I. Kolesnikov, T.E. Sherline, J.P. Clancy, K.A. Ross, J.P.C. Ruff, B. D. Gaulin, S.E. Nagler, SEQUOIA: a newly operating chopper spectrometer at the SNS, J. Phys.; Conf. Ser. 251 (2010) 012058.
[31] https://neutrons.ornl.gov/. (Accessed 9 January 2025).
[32] S.F. Parker, D. Lennon, P.W. Albers, Vibrational spectroscopy with neutrons – a review of new directions, Appl. Spec. 65 (2011) 1325–1341.
[33] S.J. Clark, M.D. Segall, C.J. Pickard, P.J. Hasnip, M.J. Probert, K. Refson, M. C. Payne, First principles methods using CASTEP, Z. Krist. 220 (2005) 567–570.
[34] J. Perdew, K. Burke, M. Ernzerhof, Generalized Gradient Approximation made simple, Phys. Rev. Lett. 77 (1996) 3865–3868.
[35] A. Tkatchenko, M. Scheffler, Accurate molecular van der Waals interactions from ground-state electron density and free-atom reference data, Phys. Rev. Lett. 102 (2009) 073005.
[36] K. Refson, P.R. Tulip, S.J. Clark, Variational density functional perturbation theory for dielectrics and lattice dynamics, Phys. Rev. B 73 (2006) 155114.
[37] X. Gonze, J.-C. Charlier, M.P. Teter, Dielectric tensor, effective charges and phonon in α-quartz by variational density functional perturbation theory, Phys. Rev. B 54 (1996) 13035–13038.
[38] BIOVIA materials studio: https://www.3ds.com/products/biovia/materials-studio Accessed on 9 January 2025.
[39] K. Dymkowski, S.F. Parker, F. Fernandez-Alonso, S. Mukhopadhyay, AbINS: the modern software for INS interpretation, Physica B 551 (2018) 443–448.
[40] Y.Q. Cheng, L.L. Daemen, A.I. Kolesnikov, A.J. Ramirez-Cuesta, Simulation of inelastic neutron scattering spectra using OCLIMAX, J. Chem. Theory Comput. 15 (2019) 1974–1982.

[41] Z. Sofer, P. Šimek, O. Jankovský, D. Sedmidubský, P. Beran, M. Pumera, Neutron diffraction as a precise and reliable method for obtaining structural properties of bulk quantities of graphene, Nanoscale 6 (2014) 13082.
[42] J.A. Read, W.K. Behl, Mechanochemical synthesis of carbon fluorides, Electrochem. Solid State Lett. 12 (2009) A16–A18.
[43] G.A. Crowder, H.K. Mao, Vibrational analysis of *n*-butyl, *n*-pentyl, and *n*-hexyl fluorides, J. Mol. Struc. 23 (1974) 161–174.
[44] V.E. Antonov, I.O. Bashkin, A.V. Bazhenov, B.M. Bulychev, V.K. Fedotov, T. N. Fursova, A.I. Kolesnikov, V.I. Kulakov, R.V. Lukashev, D.V. Matveev, M. K. Sakharov, Y.M. Shulga, Multilayer graphane synthesized under high hydrogen pressure, Carbon 100 (2016) 465–473.
[45] V.A. Yartys, V.E. Antonov, B.N. Bulychev, V.S. Efimchenko, V.I. Kulakov, M. A. Kuzovnikov, R.T. Howie, H.A. Shuttleworth, M. Holin, R. Rae, M.B. Stone, B. P. Tarasov, R.I. Usmanov, A.I. Kolesnikov, Reversible hydrogen storage in multilayer graphane: lattice dynamics, compressibility, and heat capacity studies, Mater. Chem. Phys. 332 (2025) 130232.
[46] F.A. Miller, B.M. Harney, The infrared and Raman spectra of perfluorocyclohexane, Spectrochim. Acta 28A (1972) 1059–1066.
[47] G. Masetti, F. Cabassi, G. Morelli, G. Zerbi, Conformational order and disorder in poly(tetrafluoroethylene) from the infrared spectrum, Macromolecules 6 (1973) 700–707.
[48] H. Nanaie, G.A. Guirgis, J.R. Durig, Torsional spectra of molecules with two C_{3v} rotors-XXV. Rotational and vibrational spectra, r_0 structure, barriers to internal rotation and *ab initio* calculations for 2,2-difluoropropane, Spectrochim. Acta 49A (1993) 2039–2056.
[49] P.W. Albers, W. Weber, K. Möbus, S.D. Wieland, S.F. Parker, Neutron scattering study of the terminating protons in the basic structural units of non-graphitising and graphitising carbons, Carbon 109 (2016) 239–245.
[50] A.M. Rao, A.W.P. Fung, M.S. Dresselhaus, G. Dresselhaus, M. Endo, T. Nakajima, Raman studies of fluorine-intercalated carbon fibers, MRS Online Proc. Libr. 209 (1990) 347–352.
[51] F. Tuinstra, J.L. Koenig, Raman spectrum of graphite, J. Chem. Phys. 143 (1970) 1126–1130.
[52] M. Bogojeski, L. Vogt-Maranto, M.E. Tuckerman, K.-R. Müller, K. Burke, Quantum chemical accuracy from density functional approximations via machine learning, Nature Commun 11 (2020) 5223.
[53] D.D. Chronopoulos, A. Bakandritsos, M. Pykal, R. Zbořil, M. Otyepka, Chemistry, properties, and applications of fluorographene, Appl. Mater. Today 9 (2017) 60–70.
[54] H. Peelaers, A.D. Hernández-Nieves, O. Leenaerts, B. Partoens, F.M. Peeters, Vibrational properties of graphene fluoride and graphene, Appl. Phys. Lett. 98 (2011) 051914.
[55] S.K. Sharma, R. Singh, T. D Kühne, Vibrational spectra of hydrogenated and halogenated graphene CX; X = H, F, Cl, Mater. Res. Express 6 (2019) 045612.